

Phonon thermal transport in 2H, 4H and 6H silicon carbide from first principles [☆]

Nakib Haider Protik^{a,*}, Ankita Katre^b, Lucas Lindsay^c, Jesús Carrete^d, Natalio Mingo^b,
David Broido^a

^a*Boston College, Chestnut Hill, Massachusetts 02467, USA*

^b*LITEN, CEA-Grenoble, 17 rue des Martyrs, 38054 Grenoble Cedex 9, France*

^c*Oak Ridge National laboratory, 1 Bethel Valley Rd, Oak Ridge, Tennessee 37830, USA*

^d*Institute of Materials Chemistry, TU Wien, A-1060 Vienna, Austria*

Abstract

Silicon carbide (SiC) is a wide band gap semiconductor with a variety of industrial applications. Among its many useful properties is its high thermal conductivity, which makes it advantageous for thermal management applications. In this paper we present *ab initio* calculations of the in-plane and cross-plane thermal conductivities, κ_{in} and κ_{out} , of three common hexagonal polytypes of SiC: 2H, 4H and 6H. The phonon Boltzmann transport equation is solved iteratively using as input interatomic force constants determined from density functional theory. Both κ_{in} and κ_{out} decrease with increasing n in n H SiC because of additional low-lying optic phonon branches. These optic branches are characterized by low phonon group velocities, and they increase the phase space for phonon-phonon scattering of acoustic modes. Also, for all n , κ_{in} is found to be larger than κ_{out} in the temperature range considered. At electron concentrations present in experimental samples, scattering of phonons by electrons is shown to be negligible except well below room temperature where it can lead to a significant reduction of the lattice thermal conductivity. This work highlights the power of *ab initio* approaches in giving quantitative, predictive descriptions of thermal transport in materials. It helps explain the qualitative disagreement that exists among different sets of measured thermal conductivity data and provides information of the relative quality of samples from which measured data was obtained.

Keywords: silicon carbide, thermal conductivity, phonon-phonon interaction, electron-phonon interaction, density functional theory, Boltzmann transport equation

[☆]©2017. This manuscript version is made available under the CC-BY-NC-ND 4.0 license <http://creativecommons.org/licenses/by-nc-nd/4.0/>

*Corresponding author

Email addresses: nakib.protik@bc.edu (Nakib Haider Protik), ankitamkatre@gmail.com

(Ankita Katre), lindsaylr@ornl.gov (Lucas Lindsay),
jesus.carrete.montana@tuwien.ac.at (Jesús Carrete), natalio.mingo@cea.fr (Natalio Mingo), broido@bc.edu (David Broido)

1. Introduction

The hexagonal polytypes of SiC (n H SiC with $n = 2, 4, 6$) are large, indirect band gap semiconductors. Because of their nearly three times larger band gap compared to Si, they can maintain operational performance better than Si under harsh conditions such as high temperature, high electric field intensity and frequency, high power and strong radiation. Of particular interest to us is their large lattice thermal conductivities, κ , which make them good candidates for thermal management applications. While the thermal properties of the 4H and 6H phases have been studied, there is no consensus among the various published measurements of κ [1–7]. For example, in Ref. [7] the lattice thermal conductivity parallel to the hexagonal atomic planes, κ_{in} , for the 6H phase is found to be higher than that for the 4H phase. In contrast, measured data for the 4H phase from Ref. [1] gives notably higher values than those in Ref. [7] suggesting 4H SiC has higher thermal conductivity than that of 6H SiC. In addition, even for the same n in n H SiC there is wide variation in κ values among the various measurements. Finally, phonon-electron scattering has been suggested to play a major role in lowering κ [3, 6]. However, no rigorous calculations have been performed to assess this. In this paper we address these issues by carrying out *ab initio* calculations of κ_{in} and κ_{out} in 2H, 4H and 6H SiC. We specifically answer two questions: 1) what are the trends in κ_{in} and κ_{out} among the three considered hexagonal polytypes of SiC? And, 2) how strongly does phonon-electron scattering affect κ ? We find that κ_{in} is larger than κ_{out} over a wide temperature range and that κ_{in} and κ_{out} decrease with increasing n in n H SiC. We also find

that phonon-electron scattering has a negligible effect on κ around and above room temperature, but that it can cause significant suppression of κ below around 100 K.

2. Phonon thermal transport

Phonon transport is the dominant mechanism of heat conduction in semiconductors and insulators. This is particularly true in materials such as SiC where the stiff bonding, light constituent atoms and relatively low electron concentrations make the lattice contribution to thermal conductivity much larger than that from the charge carriers. Phonon scattering due to anharmonicity (phonon-phonon scattering), structural defects, isotopes, crystal boundaries, dopants, etc. limits the thermal conductivity. An applied temperature gradient creates a non-equilibrium phonon distribution causing phonons to move diffusively through the crystal. In steady state phonon thermal transport can be described by the Peierls-Boltzmann transport equation (PBE)

$$\mathbf{v}_\lambda \cdot \nabla T \frac{\partial n_\lambda}{\partial T} = \left(\frac{\partial n_\lambda}{\partial t} \right)_{\text{collisions}}, \quad (1)$$

where $\lambda \equiv (\mathbf{q}, s)$ is the phonon mode with wavevector \mathbf{q} and polarization s , \mathbf{v}_λ is the phonon group velocity, ∇T is the applied temperature gradient, and n_λ is the non-equilibrium phonon distribution function.

For a small temperature gradient

$$n_\lambda = n_\lambda^0 + (-\partial n_\lambda^0 / \partial T) \mathbf{F}_\lambda \cdot \nabla T, \quad (2)$$

where n_λ^0 is the equilibrium phonon (Bose-Einstein) distribution. Then linearization of Eq. 1 in the assumed small ∇T gives [8, 9]

$$\mathbf{F}_\lambda = \tau_\lambda^0 (\mathbf{v}_\lambda + \mathbf{\Delta}_\lambda), \quad (3)$$

where τ_λ^0 is the total phonon mode relaxation time taking into account effects of all scatterers in the system, and Δ_λ is a linear function of \mathbf{F}_λ given by Eq. A.9 in the appendix. Eq. 3 is solved iteratively with the initial choice of $\Delta_\lambda = 0$ and by using the Matthiessen's rule: $(\tau_\lambda^0)^{-1} = \sum_i (\tau_\lambda^i)^{-1}$ where i denotes a type of phonon scatterer. This initial guess is equivalent to working in the relaxation time approximation (RTA) where both momentum conserving normal and momentum non-conserving umklapp processes are taken to be directly thermally resistive. In the iterative scheme the normal processes redistribute the phonon population while the umklapp processes remain directly thermally resistive. As a result, the iterative scheme usually produces higher thermal conductivity than predicted by the RTA [10].

Near room temperature, three-phonon scattering is the main mechanism that limits κ [11]. The three-phonon scattering rates are given by Eqs. A.3 and A.4. Phonons are also scattered by mass disorder from natural isotope mixes on Si and C atoms and from substitutional defects. The phonon-isotope scattering rates are treated using a mass-variance model [12] given by Eq. A.5. Substitutional defects, where they are considered, are also treated using the mass-variance model.

We consider phonon-electron scattering processes where phonons are either emitted or absorbed by electrons. This leads to an additional collision term on the right hand

side with Eq. 1 of the following form:

$$\left(\frac{\partial n_\lambda}{\partial t}\right)_{\text{EPI}} = \frac{4\pi}{\hbar} \sum_{mn} \sum_{\mathbf{k}} |g^{smn}(\mathbf{k}, \mathbf{q})|^2 \times \left\{ -f_{\mathbf{k}}^n (1 - f_{\mathbf{k}+\mathbf{q}}^m) n_\lambda + f_{\mathbf{k}+\mathbf{q}}^m (1 - f_{\mathbf{k}}^n) (1 + n_\lambda) \right\} \delta(\epsilon_{\mathbf{k}+\mathbf{q}}^m - \epsilon_{\mathbf{k}}^n - \hbar\omega_\lambda),$$

where m, n are electronic band indices, g is the electron-phonon interaction (EPI) matrix element, f is the electronic distribution function, ϵ is the electron energy, $(2\pi)^{-1}\omega$ is the phonon frequency and \mathbf{v} is the electron group velocity. Expanding the phonon distribution function as done in Eq. 2 while taking the electronic distribution to be in equilibrium, the phonon scattering rates due to the EPI are found in the RTA to be:

$$(\tau_\lambda^{\text{EPI}})^{-1} = \frac{4\pi}{\hbar} \sum_{mn} \sum_{\mathbf{k}} |g^{smn}(\mathbf{k}, \mathbf{q})|^2 \times \left\{ f_{\mathbf{k}}^n - f_{\mathbf{k}+\mathbf{q}}^m \right\} \delta(\epsilon_{\mathbf{k}+\mathbf{q}}^m - \epsilon_{\mathbf{k}}^n - \hbar\omega_\lambda), \quad (4)$$

where the $f \equiv f^0$ is now the equilibrium electron (Fermi-Dirac) distribution.

The lattice thermal conductivity tensor elements are calculated using

$$\kappa^{\alpha\beta} = \frac{k_B}{NV} \sum_{\lambda} \left(\frac{\hbar\omega_\lambda}{k_B T} \right)^2 n_\lambda^0 (n_\lambda^0 + 1) v_\lambda^\alpha F_\lambda^\beta, \quad (5)$$

where α, β are Cartesian directions, k_B is the Boltzmann constant, N is the total number of q -points in the Brillouin zone and V is the primitive cell volume.

3. Computational methods

Density functional theory (DFT) and density functional perturbation theory

(DFPT) calculations are performed using the Quantum ESPRESSO v. 5.4.0 suite [13]. We use a norm-conserving pseudopotential. The local density approximation with the Perdew-Zunger parametrization is chosen for the exchange-correlation functional. A variable-cell structural optimization is carried out on $8 \times 8 \times 6$, $8 \times 8 \times 4$ and $8 \times 8 \times 2$ k -meshes for the 2H, 4H and 6H structures, respectively, to find the relaxed lattice constants and atomic positions. We use DFPT to calculate the harmonic force constants and phonon dispersions. For the phonon calculations a $6 \times 6 \times 4$ q -mesh is used for the 2H phase, and $6 \times 6 \times 2$ for the 4H and 6H phases. To calculate the third order anharmonic force constants we employ a finite displacement supercell method. To generate the symmetry-allowed minimal set of two-atom-displaced supercells, extract the anharmonic force constants following Γ -point DFT calculations on said supercells, and symmetrize the force constants tensor we use the `thirdorder.py` code [8, 14]. We use a $3 \times 3 \times 3$ supercell, corresponding to 108, 216 and 324 atoms, respectively, for the 2H, 4H and 6H phases. A converged cut-off distance for the third-order force constants of 3.3 Å is used for each.

The ShengBTE software [8] is used to calculate the κ tensor using a locally adaptive Gaussian broadening method [9] to approximate the energy conserving delta functions appearing in the scattering rates expressions (see Eqs. A.10 and A.11). To keep the q -mesh spacing uniform we use $N_{x(y)}/N_z \approx b_{x(y)}/b_z$ where N is the number of sampled q -points, b is the reciprocal lattice vector component along a given Cartesian direction, and $x(y)$ and z denote Cartesian directions $\hat{x}(\hat{y})$ and \hat{z} . Given that in n H SiC $b_z < b_{x(y)}$ and in view of Eq.

A.11, it is important to keep the q -mesh spacing uniform in order to prevent the adaptive Gaussian scheme from selectively setting smaller broadening for the $(0, 0, q_z)$ modes. This causes the lowest frequency phonons to have spuriously large lifetimes. Converged q -meshes $25 \times 25 \times 15$, $23 \times 23 \times 7$ and $25 \times 25 \times 5$ were used for the κ calculations of 2H, 4H and 6H SiC, respectively.

The phonon-electron scattering rates, Eq. 4, are obtained by calculating the imaginary part of the phonon self-energy using the EPW v. 4 code [15, 16]. For the desired grid of phonon modes, the EPW code first calculates band energies and electron-phonon matrix elements *ab initio* on a coarse grid of electron wave vectors. Then, it uses maximally localized Wannier functions to interpolate the EPI matrix elements and band energies to a fine k -mesh. The original code uses a fixed Gaussian broadening to approximate delta functions; this requires convergence testing in tandem with that for the k -mesh density. We have modified the original code to employ the analytic tetrahedron method [17] which requires convergence testing only in the k -mesh density. A fine $90 \times 90 \times 60$ k -mesh is used to calculate the phonon-electron scattering rates for 2H SiC which are then combined with the other phonon scattering rates at the RTA level using Matthiessen’s rule. We checked that the calculated κ is converged with respect to the k -mesh density for the temperature range considered. Calculations for 4H and 6H SiC proved to be too computationally expensive.

4. Results and discussion

The results from structural optimization calculations are presented in Table 1. We find excellent agreement between calculated

phase	a, c (Å) theory	a, c (Å) experiment
2H	3.07, 5.04	3.08, 5.05
4H	3.07, 10.05	3.08, 10.08
6H	3.07, 15.08	3.08, 15.12

Table 1: In-plane (a) and cross-plane (c) lattice parameters of 2H, 4H and 6H SiC. Experimental results for a, c for the 2H phase are taken from Ref. [18] and for 4H and 6H from Ref. [19].

and measured [18, 19] values of the in- and cross-plane lattice constants, a and c . For the 2H SiC internal parameter we find $u(\text{C}) = 0.3754(0.375)$. For 4H SiC the internal parameters are $u(\text{C}) = 0.1874(0.1875)$ and $v(\text{Si}) = 0.25(0.25)$. And for 6H SiC: $u(\text{C}) = 0.1254(0.125)$, $v(\text{Si}) = 0.1668(0.1667)$, $v(\text{C}) = 0.2917(0.2917)$, $w(\text{Si}) = 0.333(0.333)$ and $w(\text{C}) = 0.4582(0.4583)$. The numbers in the parentheses are the ideal values for these parameters [20].

2H, 4H and 6H SiC have 4, 8, and 12 atoms per primitive unit cell, respectively, with cells becoming more elongated along the cross-plane direction of $n\text{H}$ SiC with increasing n as shown in Fig. 1. Calculated phonon dispersions for 2H, 4H and 6H SiC are shown in Fig. 2 along with available experimental measurements for 4H and 6H SiC [21–23]. The agreement between calculation and measurement is excellent.

In the 4H and 6H SiC samples considered here, substitutional nitrogen defects are present, and these can also be treated using the mass disorder model. We do not include bond-disorder arising from these substitutional defects. Here we assume that the nitrogen defects are at the carbon sites. In Fig. 3 the phonon-phonon, phonon-isotope and phonon-nitrogen defect scattering rates are shown for the 6H phase

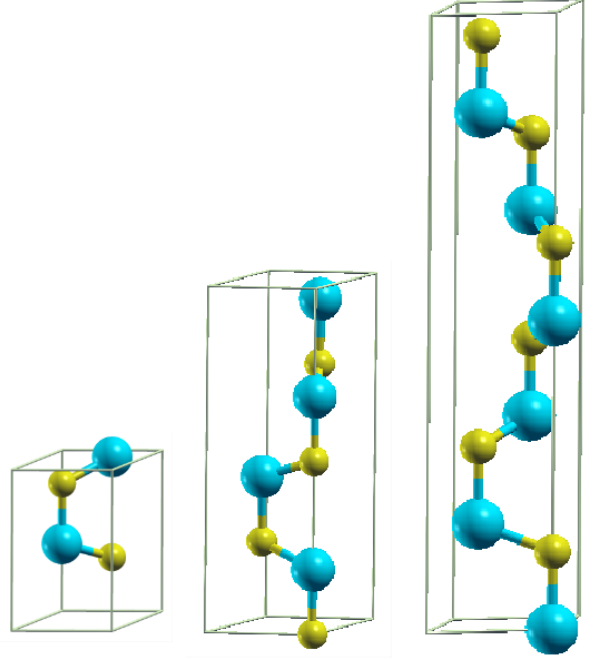
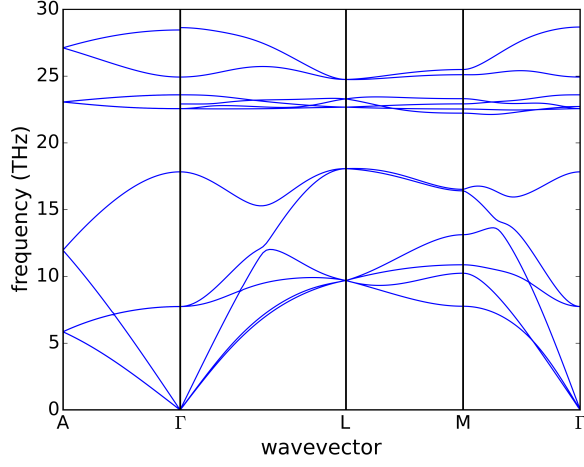
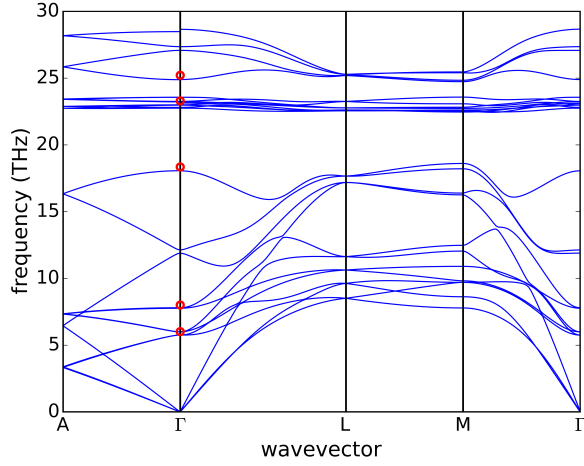


Figure 1: From left to right: 2H, 4H and 6H SiC primitive cells. Blue represents Si and yellow, C.

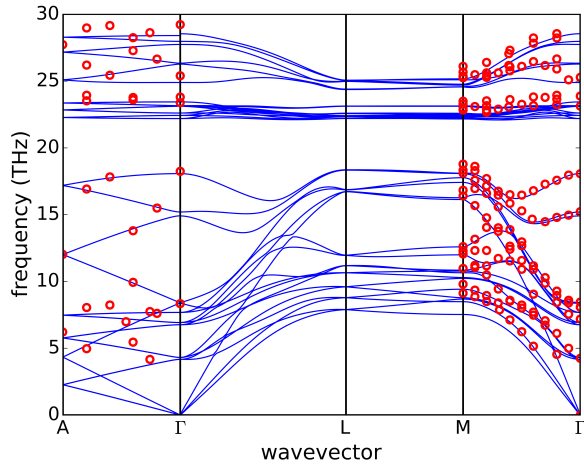
at 300 K. Phonon-phonon scattering dominates over the entire frequency range, followed by phonon-isotope scattering. The sample with the highest impurity concentration to which we compare our calculations has $2.9 \times 10^{18} \text{ cm}^{-3}$ N-atoms. Treating these as substitutional defects at the C site leads to negligible reduction in κ . This is because N defects give only a small (17%) mass increase over the C atoms, only slightly larger than that for the minority carbon isotope (^{13}C), and the N concentration is 300 times smaller than that of ^{13}C in naturally occurring carbon. The low concentration of N defects means that even if the N atoms were on the Si site instead of the C site, the phonon defect scattering rates would still be negligibly small. To support this, we note that in a recent study on cubic 3C SiC [24], N substitution defects at the C site were treated as both mass and bond defects. For the



(a)



(b)



(c)

Figure 2: Phonon dispersions of (a) 2H, (b) 4H and (c) 6H SiC. Blue curves are calculated results. Red circles are from experimental measurements for 4H [21] and 6H [22] phases, respectively.

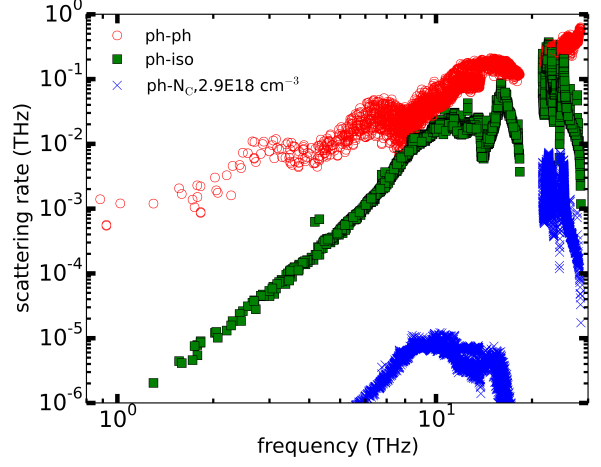


Figure 3: Phonon-phonon, phonon-isotope and phonon-N-substitution scattering rates for 6H SiC at 300 K. N substitution is considered at the C site with a concentration of $2.9 \times 10^{18} \text{ cm}^{-3}$ matching the highest N-doped sample in Ref. [3].

N-doping concentrations considered in the present work, a negligible reduction in the κ of 3C SiC was found around 300 K. For all κ calculations phonon-isotope scattering is included, while phonon-substitution defect scattering is ignored for the remaining results presented.

Fig. 4 shows the calculated temperature dependence of κ_{in} and κ_{out} for the three polytypes considered. For both in-plane and cross-plane directions, we find that $\kappa_{2\text{H}} > \kappa_{4\text{H}} > \kappa_{6\text{H}}$. This is explained by the fact that in these hexagonal polytypes the larger number of atoms with increasing n in $n\text{H}$ SiC gives rise to an increasing number of low-lying optic branches. The small phonon group velocities in these branches combined with the fact that the three-phonon scattering rates are the highest in 6H SiC and the lowest in 2H SiC leads to lower κ with increasing n in $n\text{H}$ SiC. Also, for given n in $n\text{H}$ SiC, we find that $\kappa_{\text{in}} > \kappa_{\text{out}}$ over the temperature range considered. This anisotropy arises from larger contributions

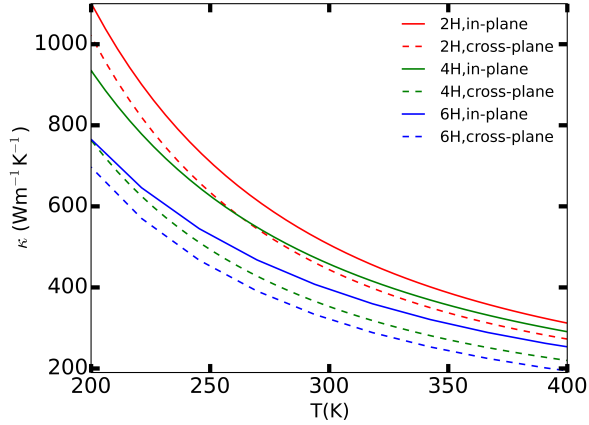


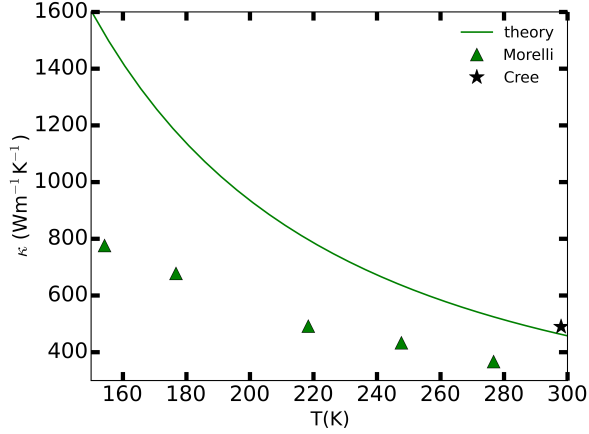
Figure 4: Temperature dependence of κ_{in} and κ_{out} for 2H, 4H and 6H SiC. For a given direction, $\kappa_{2H} > \kappa_{4H} > \kappa_{6H}$. For both the solid and dashed types, the top (middle) [bottom] line corresponds to 2H (4H) [6H] SiC κ .

to the in-plane thermal conductivity integral, Eq. 5, from the $v_{\lambda}^x F_{\lambda}^x$ terms compared to those for the corresponding cross-plane (z) components, especially in the frequency range around 10 THz. Roughly the same anisotropy is found in both the RTA and the iterated calculations.

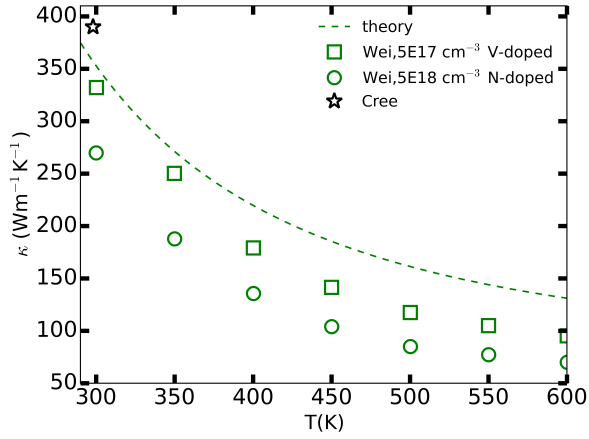
In Fig. 5 (a) the calculated κ_{in} of 4H SiC are compared to experimental data. Green triangles give κ_{in} measured by Morelli et al. [7]. These data points lie well below the calculated κ_{in} values (solid green curve). The authors in Ref. [7] speculate that their 4H sample may have stacking faults. These types of defects are not treated in our theoretical framework, and we attribute the large difference between calculation and the data from Ref. [7] to the presence of such defects. On the other hand, a measurement of κ_{in} by Cree Inc. [1] (black filled symbol) on their high purity semi-insulating sample at 298 K shows good agreement with the calculated κ_{in} . Specifically, we calculated $\kappa_{\text{in}} = 451 \text{ Wm}^{-1}\text{K}^{-1}$, only 8% smaller than the measured Cree value of $490 \text{ Wm}^{-1}\text{K}^{-1}$.

Fig. 5 (b) shows the calculated results for κ_{out} (green dashed curve) compared to measured data from Wei et al. [6] and that from Cree [1]. The sample with higher κ_{out} from Ref. [6] was believed to contain $5 \times 10^{17} \text{ cm}^{-3}$ vanadium substitutional defects while that with the lower κ_{out} contained $5 \times 10^{18} \text{ cm}^{-3}$ nitrogen substitutional defects. Treating the V and N dopants as substitutional defects at the C site lead to negligible reduction of κ . The measurements near room temperature from the less doped samples of Ref. [6] and from Ref. [1] are in good agreement with the calculated results. However, at higher temperatures, both sets of measured data from Ref. [6] lie well below our calculated values. This is puzzling to us. Moreover, the measured κ values for the sample with the higher defect/carrier density are significantly smaller than those for the lower defect/carrier density sample even though the calculated phonon-defect scattering rates in both cases are small and phonon-electron scattering in this temperature range is weak (see discussion below). Finally, the measured κ values for both samples saturate above 600 K, a finding inconsistent with the roughly $1/T$ dependence of the thermal conductivity from phonon-phonon scattering and the expected negligible contribution from the electronic part of the thermal conductivity.

In Fig. 6 we compare κ_{in} of 6H SiC with measurements from Slack [2], Morelli et al. [3] and Burgemeister et al. [4]. Calculated values (solid blue line) lie below the Slack data (purple squares) with N defect concentration of $1 \times 10^{17} \text{ cm}^{-3}$, but above the data from Morelli et al. whose samples had N concentrations of 3.5×10^{16} and $2.9 \times 10^{18} \text{ cm}^{-3}$, respectively. For the sparsely doped Morelli sample (blue triangles) agreement with theory is very good between 200 and



(a)



(b)

Figure 5: Comparison of the calculated 4H SiC (a) κ_{in} and (b) κ_{out} with experimental measurements from [7] (green triangles), [6] (green open squares and circles) and [1] (black open stars).

300 K - at 150 K the calculated value is about 20% larger than the experimental one. For the higher doped Morelli sample (blue circles) the measured κ_{in} is significantly lower than the calculated values. This reduction is attributed by Morelli et al. to phonons scattering from electrons donated by N atoms. The Burgemeister data points (black symbols) are measurements above 300 K for lightly N- or p-type doped samples. There is some variation in

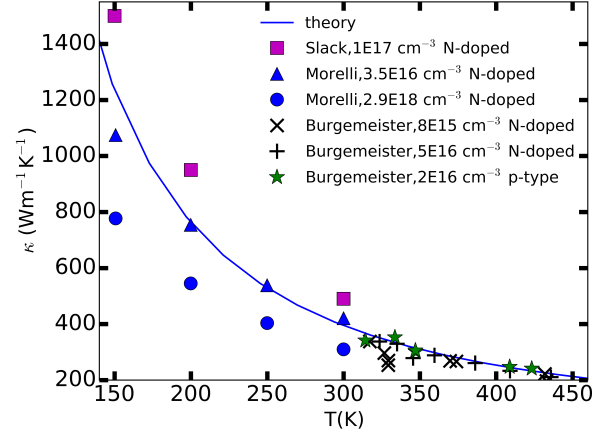


Figure 6: Comparison of the calculated 6H SiC κ_{in} with measured data from Ref. [2] (purple squares), Ref. [3] (blue triangles and circles) and Ref. [4] (green stars, black crosses and black pluses).

the measured data, but in general the trend is well captured by the theory curve. We note that the $8 \times 10^{15} \text{ cm}^{-3}$ N-doped Burgemeister data points (black cross symbols) slightly above 300 K show a variation nearly equal to the difference between the nearest Morelli data points. Moreover, the Slack sample with nearly 3 times the N-doping of the the purest Morelli sample has a significantly higher κ_{in} than the latter and also projects to larger κ_{in} than the higher purity samples of Burgemeister. The reason for the high measured κ_{in} for the Slack sample is unclear to us. It is also unclear whether the difference between the κ measurement on the two Morelli samples is entirely due to the EPI.

In Fig. 7 the calculated κ_{out} of 6H SiC is compared to experimental data from Nilsson et al. [5] between 300 and 2300 K. Also plotted are κ_{out} measurements by Burgemeister et al. [4]. Excellent agreement between calculation and data from Refs. [5] and [4] is found in this case over the entire temperature range of the data. We note that even at high temperatures the thermal

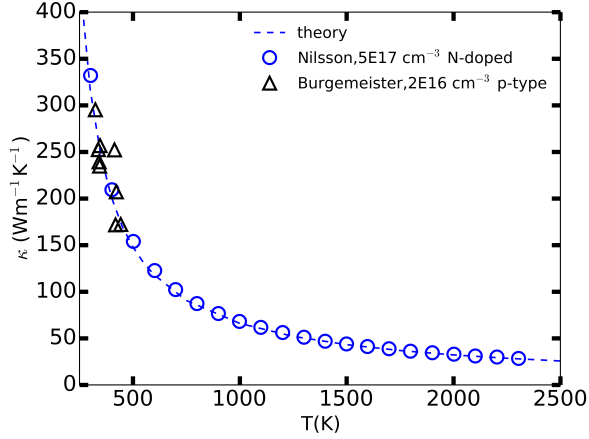


Figure 7: Comparison of 6H SiC κ_{out} with experimental measurements from Refs. [5] (blue open circles) and [4] (black open triangles).

expansion coefficient of 6H SiC is almost independent of temperature [25], which suggests that higher-order anharmonicity is weak even at the high temperatures (up to 2300K) of the measurements of Ref. [5].

The experimental sample from Ref. [5] has an N-doping concentration of $5 \times 10^{17} \text{ cm}^{-3}$. At 300 K the measured κ value is 4.1% higher than the calculated value. Interestingly, while the EPI was thought to give a significant reduction in κ_{in} in Ref. [3], [4], [7] even at 300K, such a reduction is not seen by comparing the 300 K κ_{out} data from Nilsson and Burgemeister in spite of there being an order of magnitude difference in carrier densities. Instead the two sets of κ_{out} measured values are quite close to each other and are also in very good agreement with the theoretical results.

To address the question of to what extent the EPI reduces κ we calculated phonon-electron scattering rates for the 2H phase. Full first principles treatment of the EPI in 4H and 6H SiC is currently beyond our computational capabilities. In Fig. 8 phonon-electron scattering rates for 2H SiC for a

representative electron density of 10^{18} cm^{-3} are plotted along with phonon-phonon and phonon-isotope scattering rates at 300 K. The phonon-electron scattering rates are shown here on a dense q -mesh of $50 \times 50 \times 30$ to highlight their frequency dependence while the other scattering rates are shown on the originally converged $25 \times 25 \times 15$ q -mesh. In the low frequency region the acoustic-phonon-electron scattering rates are comparable to the phonon-phonon scattering rates before quickly falling off above 2 THz. The phonon-electron scattering rates become strong again for the high optic phonon frequencies. The high-lying optic phonons contribute negligibly to κ , as can be seen from the spectral contribution to κ_{in} ($\kappa_{\text{in}}(\nu)$) [26] for 2H and 6H SiC shown in Fig. 9. Therefore, strong phonon-electron scattering for those phonons will not affect κ . It is seen in Fig. 9 that the effect of phonon-electron scattering in suppressing the κ_{in} of 2H SiC is only visible below around 3 THz. For example, at 1 THz, $\kappa_{\text{in}}(\nu)$ is suppressed by about 39%, but beyond 3 THz there is no suppression. At higher temperatures above 300 K phonon-phonon scattering dominates over all other scattering mechanisms and the effect of the EPI is predicted here to be negligible. However, at lower temperatures, phonon-phonon scattering weakens and the reduction in κ due to phonon-electron scattering can become significant.

The effect of the EPI on 2H SiC κ_{in} is presented in Table 2 for 10^{17} cm^{-3} and 10^{18} cm^{-3} n-type doping concentrations. For 10^{17} cm^{-3} doping concentration we see a 20% reduction of κ_{in} at 100 K while the reductions at 300 K and 600 K are negligible. For 10^{18} cm^{-3} doping concentration these numbers are 28%, 4.4% and 1.1%, respectively. These results are consistent with the

discussion in the previous paragraph.

Table 3 compares the calculated undoped κ_{in} for 6H SiC with the corresponding measured values from Ref. [3] for the sample with electron density of $2.9 \times 10^{18} \text{ cm}^{-3}$. Assuming that the strength of the EPI in 6H SiC is similar to that in 2H SiC and coupling this to the fact that phonon-phonon scattering is stronger in 6H SiC than in 2H SiC we conclude that the EPI is not likely the only reason for the strong reduction in κ in Ref. [3], nor can it be the sole explanation for the difference in thermal conductivities of the 6H samples from Ref. [2] (see Fig. 6) or the 4H samples from Ref. [6] (see Fig. 5b).

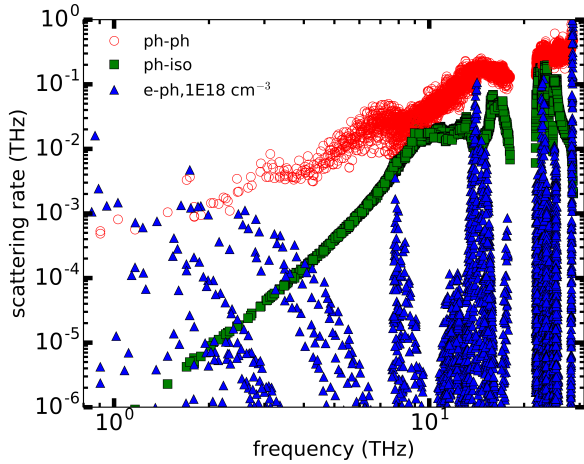


Figure 8: Phonon-electron scattering rates in 2H SiC at 300 K for an electron concentration of 10^{18} cm^{-3} . For comparison, phonon-phonon and phonon-isotope scattering rates are also plotted.

5. Conclusion

We have presented *ab initio* calculations of the in-plane and cross-plane lattice thermal conductivities, κ_{in} and κ_{out} , for 2H, 4H and 6H SiC. We found that for both in-plane and cross-plane thermal transport, the 2H phase has the highest κ , followed by that of

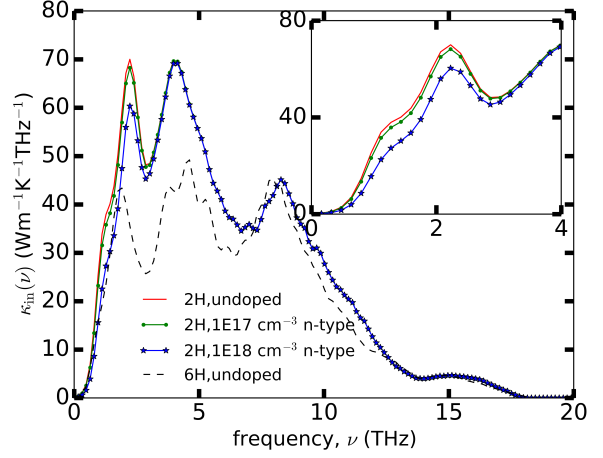


Figure 9: Spectrum of κ_{in} as a function of frequency ν for 2H and 6H SiC at 300 K. Effect of EPI is shown for 2H for two n-type doping levels. The inset plot zooms in on the [0,4] THz region.

T(K)	undoped	n-type 10^{17} cm^{-3}	n-type 10^{18} cm^{-3}
100	4741	3779, (20%)	3398, (28%)
300	497	492, (1.0%)	475, (4.4%)
600	186	185, (0.5%)	184, (1.1%)

Table 2: Calculated 2H SiC κ_{in} ($\text{Wm}^{-1}\text{K}^{-1}$) with and without the EPI. The third and fourth columns give κ_{in} , percentage reduction with respect to the undoped case.

4H SiC and then by that of 6H SiC. Also, for given n in $n\text{H}$ SiC, κ_{in} is found to be larger than κ_{out} over a large range of temperatures. Reasonably good agreement is obtained with the measured κ_{in} and κ_{out} results for some of the 4H and 6H samples. However, wide variations in measured data were noted that in most cases suggest the presence of defects in the measured samples. By calculating phonon-electron scattering from first principles for the 2H phase at electron densities representative of those in the studied samples, we concluded that such scattering is not likely the sole reason for the difference in κ measurements between

T(K)	undoped (theory)	N-doped $2.9 \times 10^{18} \text{ cm}^{-3}$
100	2460	1018, (59%)
300	382	310, (19%)

Table 3: 6H SiC κ_{in} ($\text{Wm}^{-1}\text{K}^{-1}$) values from theory (undoped, column 2) .vs. experiment (N-doped, column 3) [3]. The third column also shows percentage difference between the calculated and measured κ_{in} .

the 6H SiC samples considered in Ref. [3] or for the difference between the measured κ values for the 4H SiC samples in Ref. [6]. Nevertheless, carrier concentrations as low as $1 \times 10^{18} \text{ cm}^{-3}$ in the 2H phase can lead to a significant reduction in κ at low temperatures, which is qualitatively consistent with the measurement findings [3].

Acknowledgements

N.H.P. and D.B. acknowledge support from the Office of Naval Research MURI, Grant No. N00014-16-1-2436 and from the Pleiades computational cluster of Boston College. This work used the Extreme Science and Engineering Discovery Environment (XSEDE) [27], which is supported by National Science Foundation grant number ACI-1548562. N.H.P. acknowledges help from Dr. Chunhua Li with EPW calculations. L.L. acknowledges support from the U.S. Department of Energy, Office of Science, Office of Basic Energy Sciences, Materials Sciences and Engineering Division. AK and NM acknowledge support from the Air Force Office of Scientific Research, USAF under award No. FA9550615-1-0187 DEF.

Appendix A.

In this appendix we provide the expressions for the phonon-phonon and phonon-mass defect scattering rates.

Three phonon scattering processes satisfy the following quasimomentum and energy conservation relations

$$\mathbf{q} \pm \mathbf{q}' + \mathbf{G} = \mathbf{q}''$$

$$\omega_{\lambda} \pm \omega_{\lambda'} = \omega_{\lambda''}, \quad (\text{A.1})$$

where \mathbf{G} a the reciprocal lattice vector.

For the \pm processes defined in A.1 the three phonon scattering matrix elements are given by

$$\Phi_{\lambda\lambda'\lambda''}^{\pm} = \sum_{\langle i \rangle jk} \sum_{\alpha\beta\gamma} \Psi_{ijk}^{\alpha\beta\gamma} \frac{e^{i\alpha} e_{s,\mathbf{q}}^{j\beta} e_{s',\pm\mathbf{q}'}^{k\gamma} e_{s'',-\mathbf{q}''}^{k\gamma}}{\sqrt{m_i m_j m_k}}, \quad (\text{A.2})$$

where i, j, k label atoms in the supercell with $\langle i \rangle$ symbolizing restricted sum over the primitive cell, m_i is the mass of atom i , $e_{s,\mathbf{q}}^{i\alpha}$ is the α Cartesian component of the phonon eigenvector associated with polarization s and wavevector \mathbf{q} , and $\Psi_{ijk}^{\alpha\beta\gamma} = \frac{\partial^3 U}{\partial r_i^{\alpha} \partial r_j^{\beta} \partial r_k^{\gamma}}$ is the third-order anharmonic force constant where r_i^{α} is the displacement of atom i in the Cartesian direction α calculated from the crystal potential energy U .

In terms of the scattering matrix elements the three phonon scattering rates of single processes are

$$W_{\lambda\lambda'\lambda''}^{+} = \frac{\hbar\pi}{4} \frac{n_{\lambda'}^0 - n_{\lambda''}^0}{\omega_{\lambda}\omega_{\lambda'}\omega_{\lambda''}} |\Phi_{\lambda\lambda'\lambda''}^{+}|^2$$

$$\times \delta(\omega_{\lambda} + \omega_{\lambda'} - \omega_{\lambda''}), \quad (\text{A.3})$$

$$W_{\lambda\lambda'\lambda''}^{-} = \frac{\hbar\pi}{4} \frac{n_{\lambda'}^0 + n_{\lambda''}^0 + 1}{\omega_{\lambda}\omega_{\lambda'}\omega_{\lambda''}} |\Phi_{\lambda\lambda'\lambda''}^{-}|^2$$

$$\times \delta(\omega_{\lambda} - \omega_{\lambda'} - \omega_{\lambda''}). \quad (\text{A.4})$$

Phonon-mass defect scattering rates for single processes are given by

$$W_{\lambda\lambda'} = \frac{\pi}{2} \omega_{\lambda}^2 \sum_i g_i |\mathbf{e}_{i\lambda}^* \cdot \mathbf{e}_{i\lambda'}|^2 \delta(\omega_{\lambda} - \omega_{\lambda'}), \quad (\text{A.5})$$

where i labels an atom in the primitive cell and

$$g_i = \sum_t f_{ti} \left(\frac{\Delta m_{ti}}{\bar{m}_i} \right)^2 \quad (\text{A.6})$$

is the mass variance parameter for atom i , with $\Delta m_{ti} \equiv m_{ti} - \bar{m}_i$ and t denoting the type of mass defect (eg. isotope, substitutional defect) at site i . \bar{m}_i is the average mass of the atom i and f_{ti} , the fraction of atoms of type t at the site i .

In the RTA the total phonon scattering rates including phonon-phonon and phonon-mass defect scattering are

$$(\tau_\lambda^{\text{anh}})^{-1} = \frac{1}{N} \left(\sum_{\lambda'\lambda''}^+ W_{\lambda\lambda'\lambda''}^+ + \frac{1}{2} \sum_{\lambda'\lambda''}^- W_{\lambda\lambda'\lambda''}^- \right) \quad (\text{A.7})$$

$$(\tau_\lambda^{\text{mass}})^{-1} = \frac{1}{N} \sum_{\lambda'} W_{\lambda\lambda'}, \quad (\text{A.8})$$

where N is the total number of points in the Γ -centered, regular q -mesh sampling the Brillouin zone and the \pm on the summation symbolize conservation restrictions given by A.1. And finally, the function Δ appearing in the linearized PBE is given by

$$\Delta_\lambda = \frac{1}{N\omega_\lambda} \left\{ \sum_{\lambda'\lambda''}^+ W_{\lambda\lambda'\lambda''}^+ (\omega_{\lambda''} \mathbf{F}_{\lambda''} - \omega_{\lambda'} \mathbf{F}_{\lambda'}) + \frac{1}{2} \sum_{\lambda'\lambda''}^- W_{\lambda\lambda'\lambda''}^- (\omega_{\lambda''} \mathbf{F}_{\lambda''} + \omega_{\lambda'} \mathbf{F}_{\lambda'}) \right\}. \quad (\text{A.9})$$

The energy conserving delta functions appearing in equations above are approximated in ShengBTE using a Gaussian function

$$\delta(\omega_\lambda - \omega) \approx \frac{1}{\sqrt{2\pi}\sigma_\omega} \exp \left[-\frac{(\omega_\lambda - \omega)^2}{2\sigma_\omega^2} \right], \quad (\text{A.10})$$

where σ_ω is a locally adaptive broadening parameter found using

$$\sigma_\omega \approx \frac{1}{\sqrt{12}} \sqrt{\sum_\mu \left[(\mathbf{v}_{\lambda'} - \mathbf{v}_{\lambda''}) \cdot \frac{\mathbf{Q}_\mu}{N_\mu} \right]^2}, \quad (\text{A.11})$$

where \mathbf{Q}_μ is the reciprocal lattice vector in the direction μ , \mathbf{v}_λ is the Cartesian group velocity of the phonon mode λ , and N_μ is the number of grid points used along the reciprocal lattice vector \mathbf{Q}_μ . In $n\text{H SiC}$, $Q_3 < Q_{1(2)}$. If the same $N_\mu = N$ is used for all three directions then $Q_3/N < Q_{1(2)}/N$. As a result Γ -A phonon modes, for which $\mathbf{q} = (0, 0, q_z)$, will have selectively smaller σ_ω compared to other modes. This is why N_μ must be chosen such that the grid spacing along all three directions is uniform.

References

- [1] Cree silicon carbide substrates and epitaxy, http://www.wolfspeed.com/index.php/downloads/dl/file/id/888/product/0/materials_catalog.pdf.
- [2] G. A. Slack, Thermal conductivity of pure and impure silicon, silicon carbide, and diamond, *Journal of Applied Physics* 35 (12) (1964) 3460–3466.
- [3] D. T. Morelli, J. P. Heremans, C. P. Beetz, W. S. Yoo, H. Matsunami, Phonon-electron scattering in single crystal silicon carbide, *Applied Physics Letters* 63 (23) (1993) 3143–3145.
- [4] E. A. Burgemeister, W. Von Muench, E. Pattenpaul, Thermal conductivity and electrical properties of 6H silicon carbide, *Journal of Applied Physics* 50 (9) (1979) 5790–5794.
- [5] O. Nilsson, H. Mehling, R. Horn, J. Fricke, R. Hofmann, S. G. Müller, R. Eckstein, D. Hofmann, Determination of the thermal diffusivity and conductivity of monocrystalline silicon carbide (300–2300 K), *High Temperatures. High Pressures* 29 (1) (1997) 73–79.
- [6] R. Wei, S. Song, K. Yang, Y. Cui, Y. Peng, X. Chen, X. Hu, X. Xu, Thermal conductivity

- of 4H-SiC single crystals, *Journal of Applied Physics* 113 (5) (2013) 053503.
- [7] D. T. Morelli, J. P. Heremans, C. P. Beetz, W. S. Yoo, G. Harris, T. C. Carrier concentration dependence of the thermal conductivity of silicon carbide, *Institute of Physics Conference Series* (137) (1993) 313–316.
- [8] W. Li, J. Carrete, N. A. Katcho, N. Mingo, ShengBTE: a solver of the Boltzmann transport equation for phonons, *Comp. Phys. Commun.* 185 (2014) 17471758. doi:10.1016/j.cpc.2014.02.015.
- [9] W. Li, N. Mingo, L. Lindsay, D. A. Broido, D. A. Stewart, N. A. Katcho, Thermal conductivity of diamond nanowires from first principles, *Phys. Rev. B* 85 (2012) 195436.
- [10] M. Omini, A. Sparavigna, An iterative approach to the phonon boltzmann equation in the theory of thermal conductivity, *Physica B: Condensed Matter* 212 (2) (1995) 101–112.
- [11] J. M. Ziman, *Electrons and phonons: the theory of transport phenomena in solids*, Oxford university press, 1960.
- [12] S.-i. Tamura, Isotope scattering of dispersive phonons in Ge, *Physical Review B* 27 (2) (1983) 858.
- [13] P. Giannozzi, S. Baroni, N. Bonini, M. Calandra, R. Car, C. Cavazzoni, D. Ceresoli, G. L. Chiarotti, M. Cococcioni, I. Dabo, et al., Quantum espresso: a modular and open-source software project for quantum simulations of materials, *Journal of physics: Condensed matter* 21 (39) (2009) 395502.
- [14] W. Li, L. Lindsay, D. A. Broido, D. A. Stewart, N. Mingo, Thermal conductivity of bulk and nanowire $\text{Mg}_2\text{Si}_x\text{Sn}_{1-x}$ alloys from first principles, *Phys. Rev. B* 86 (2012) 174307.
- [15] S. Poncé, E. R. Margine, C. Verdi, F. Giustino, EPW: Electron-phonon coupling, transport and superconducting properties using maximally localized wannier functions, *Computer Physics Communications* 209 (2016) 116–133.
- [16] F. Giustino, M. L. Cohen, S. G. Louie, Electron-phonon interaction using wannier functions, *Physical Review B* 76 (16) (2007) 165108.
- [17] P. Lambin, J. Vigneron, Computation of crystal green’s functions in the complex-energy plane with the use of the analytical tetrahedron method, *Physical Review B* 29 (6) (1984) 3430.
- [18] H. Schulz, K. H. Thiemann, Structure parameters and polarity of the wurtzite type compounds SiC₂H and ZnO, *Solid State Communications* 32 (9) (1979) 783–785.
- [19] M. Stockmeier, R. Müller, S. Sakwe, P. Wellmann, A. Magerl, On the lattice parameters of silicon carbide, *Journal of Applied Physics* 105 (3) (2009) 033511.
- [20] P. Käckell, B. Wenzien, F. Bechstedt, Electronic properties of cubic and hexagonal SiC polytypes from ab initio calculations, *Physical Review B* 50 (15) (1994) 10761.
- [21] D. W. Feldman, J. H. Parker Jr, W. J. Choyke, L. Patrick, Phonon dispersion curves by raman scattering in SiC, polytypes 3C, 4H, 6H, 15R, and 21R, *Physical Review* 173 (3) (1968) 787.
- [22] S. Nowak, Crystal lattice dynamics of various silicon-carbide polytypes, in: *International Conference on Solid State Crystals 2000, International Society for Optics and Photonics*, 2001, pp. 181–186.
- [23] To our knowledge, there is no measured phonon data for 2H SiC.
- [24] A. Katre, J. Carrete, B. Dongre, G. K. Madsen, N. Mingo, Exceptionally strong phonon scattering by B substitution in cubic SiC, arXiv preprint arXiv:1703.04996.
- [25] A. Taylor, R. Jones, Silicon carbide-a high temperature semiconductor, in: *Proc. Conf. on Silicon Carbide* (Boston, MA 1959), 1960, pp. 147–54.
- [26] The spectrum of $\kappa^{\alpha\beta}$ is given by $\kappa^{\alpha\beta}(\nu) = \frac{k_B}{NV} \sum_{\lambda} \left(\frac{\hbar\omega_{\lambda}}{k_B T} \right)^2 n_{\lambda}^0 (n_{\lambda}^0 + 1) v_{\lambda}^{\alpha} F_{\lambda}^{\beta} \delta(\nu - \nu_{\lambda})$, where $(2\pi)^{-1}\nu$ is the frequency.
- [27] J. Towns, T. Cockerill, M. Dahan, I. Foster, K. Gaither, A. Grimshaw, V. Hazlewood, S. Lathrop, D. Lifka, G. D. Peterson, et al., XSEDE: accelerating scientific discovery, *Computing in Science & Engineering* 16 (5) (2014) 62–74.